Check for updates

Geophysical Research Letters

RESEARCH LETTER
10.1029/2024GL109612

Upper Limit of Outer Belt Electron Acceleration and Their Controlling Geomagnetic Conditions: A Comparison of Storm and Non-Storm Events

Man Hua[1] **and Jacob Bortnik**[1]

[1]Department of Atmospheric and Oceanic Sciences, UCLA, Los Angeles, CA, USA

Key Points:

- Electron acceleration frequently occurs both at <2 MeV at $L < 4.0$ and at multi-MeV at $L > 4.5$, with stronger acceleration confined to $L > \sim 4.0$
- Upper limit of electron acceleration regardless of storms is governed by the cumulative impact of substorms measured by time-integrated AL
- Intense storm with lower electron density and plasmapause compared to non-storm favors but is not required to produce large maximum fluxes

Supporting Information:

Supporting Information may be found in the online version of this article.

Correspondence to:

M. Hua,
manhua@ucla.edu

Citation:

Hua, M., & Bortnik, J. (2024). Upper limit of outer belt electron acceleration and their controlling geomagnetic conditions: A comparison of storm and non-storm events. *Geophysical Research Letters*, *51*, e2024GL109612. https://doi.org/10.1029/2024GL109612

Received 2 APR 2024
Accepted 21 JUN 2024

© 2024. The Author(s).
This is an open access article under the terms of the Creative Commons Attribution License, which permits use, distribution and reproduction in any medium, provided the original work is properly cited.

Abstract We perform a comprehensive investigation of the statistical distribution of outer belt electron acceleration events over energies from 300 keV to ~10 MeV regardless of storm activity using 6-years of observations from Van Allen Probes. We find that the statistical properties of acceleration events are consistent with the characteristic energies of combined local acceleration by chorus waves and inward radial diffusion. While electron acceleration events frequently occur both at <2 MeV at $L < 4.0$ and at multi-MeV at $L > 4.5$, significant acceleration events are confined to $L > \sim 4.0$. By performing superposed epoch analysis of acceleration events during storm and non/weak storm events and comparing their geomagnetic conditions, we reveal the strong correlation (>0.8) between accumulated impacts of substorms as measured by time-integrated AL (Int(AL)) and the upper flux limit of electron acceleration. While intense storms can provide favorable conditions for efficient acceleration, they are not necessarily required to produce large maximum fluxes.

Plain Language Summary The Earth's outer belt electrons with high energies, also known as "killer" electrons due to their deleterious effects on satellites, can be quickly accelerated with fluxes varying up to several orders of magnitude. Historically, these electron dynamics are associated with geomagnetic storms. It remains unclear what is the critical geomagnetic condition that governs the electron acceleration during non/weak storm time. Our study, to our best knowledge, provides the first statistical analysis of electron acceleration events over a wide energy range (300 keV to ~10 MeV) regardless of storm events using 6-years observations from Van Allen Probes. The statistical properties of acceleration events strongly depend on L-shell and energy, which are consistent with the characteristic energies of combined local acceleration by chorus waves and inward radial diffusion. By performing a superposed epoch analysis of acceleration events during storm and non/weak storm events and comparing their geomagnetic conditions, we reveal the strong correlation between accumulated impacts of substorms as indicated by time-integrated AL (Int(AL)) and the upper limit of electron acceleration. While intense storms can provide favorable conditions for efficient acceleration, they are not necessarily required to produce large maximum fluxes.

1. Introduction

The Earth's outer radiation belt electrons contain energies ranging from 100s keV to several MeV, and can pose a hazard to the Earth-orbiting satellites as well as our heavily space-based connection-dependent society. These electrons can be quickly accelerated, with fluxes varying by several orders of magnitude on timescales of hours to days via local acceleration by whistler-mode chorus waves (e.g., Reeves et al., 2013; Thorne et al., 2013) and inward radial diffusion (e.g., Hudson et al., 2008; Ozeke et al., 2020). Nevertheless, recent statistical studies reported the existence of an upper limit for these electron fluxes during storm time, showing similar energy spectra shapes regardless of storm magnitude, with shaper gradients at multi-MeV compared to hundreds of keV (Hua, Bortnik, & Ma, 2022; Zhang et al., 2021). The key question to address, is: what is the critical geomagnetic condition that produces larger electron maximum fluxes at this upper limit? It is crucial to understand the underlying physical mechanisms that control these electron dynamics and is the primary concern in radiation belt electron forecast.

Several efforts have been dedicated to understanding the critical factors in producing upper limit of electron fluxes. Statistical studies demonstrated a small correlation between maximum fluxes and magnitude of storms as measured by averaged Dst, $(\text{SYM-H})_{\text{min}}$, or time-integral of SYM-H indices (Hua, Bortnik, & Ma, 2022, Hua et al., 2019; Zhang et al., 2021), indicating that the maximum electron fluxes are not dominantly controlled by storm activity or intensity. By comparing electron dynamics during small and large storms, Anderson et al. (2015)

19448007, 2024, 13, Downloaded from https://agupubs.onlinelibrary.wiley.com/doi/10.1029/2024GL109612, Wiley Online Library on [25/05/2025]. See the Terms and Conditions (https://onlinelibrary.wiley.com/terms-and-conditions) on Wiley Online Library for rules of use; OA articles are governed by the applicable Creative Commons License

demonstrated that the response of relativistic electrons at geosynchronous orbit to small storms is as extreme as large storms. By separately investigating the impacts of storms and substorms, Hua, Bortnik, Chu, et al. (2022) revealed the essential role of cumulative substorm activity as indicated by the time-integral of AL index instead of storms in producing the maximum fluxes during storm time, which is supported by the results using machine-learning technique, indicating the significant contributions of clusters of AL peaks to the rapid flux enhancement (Ma et al., 2024). This is mainly attributed to the sustained existence of both source and seed electrons during intense and long-lasting substorms (Hua, Bortnik, Spence, & Reeves, 2023; Jaynes et al., 2015). Their results are consistent with previous studies that time-integrated geomagnetic indices were more informative in predicting the 10-day time-integrated 2-MeV electron acceleration in the outer belt than instantaneous values (Mourenas et al., 2019, 2022). The reason is that the upper limit of relativistic electron fluxes are the cumulative results of acceleration processes that take hours to days to reach their full effect (Agapitov et al., 2019; Li et al., 2016; Tu et al., 2014).

Although previous studies have revealed the crucial role of the time-integrated substorm activity in producing the maximum fluxes, all of these studies are limited to electron acceleration during storm events while it remains unclear whether this conclusion applies to non/weak storm events. Furthermore, historically, relativistic electron dynamics has been associated with storm activities (e.g., Murphy et al., 2018; O'Brien et al., 2001; Reeves, 1998; Reeves et al., 2003). This is reflected in that the most popular way of investigating the outer belt electron dynamics is to perform superposed epoch analysis with $t_{epoch} = 0$ corresponding to $(SYM\text{-}H)_{min}$ (e.g., Gu et al., 2020; Turner et al., 2015, 2019; Zhao et al., 2019). Considering that the upper limit of electron fluxes does not depend on storms, a comprehensive study is needed to investigate the upper limit of electron acceleration during both storm and non-storm events, and compare their critical controlling geomagnetic conditions. In this letter, for the first time, we investigate the statistical distributions of outer belt electron acceleration events over energies of 300 keV–10 MeV regardless of storm activity during the Van Allen Probes Era. By comparing the electron flux evolution during storm and non-storm events and performing correlation analysis, we aim to identify the controlling geomagnetic conditions needed to reach the upper limit of outer belt electron acceleration during both storm and non-storm time.

2. Selection of Outer Belt Electron Acceleration Events

In this study, we employed electron flux data from the Energetic Particle Composition and Thermal Plasma suite (ECT; Spence et al., 2013) onboard both Van Allen Probes (Mauk et al., 2013) during 2013–2018. The spin-averaged cross-calibrated fitted electron flux data product with high energy resolution were adopted (Boyd et al., 2019). The L-shell used in this study is the McIlwain L calculated using the TS04D model (Tsyganenko & Sitnov, 2005). We adopted the storm index (SYM-H) and substorm index (AL) at 1-min resolution from the OMNI data set.

To comprehensively examine the statistical distributions of outer belt electron acceleration events and their upper limit, we analyze all the electron acceleration events across energies of 300 keV–10 MeV over $L = 2.0$–6.5 during 2013–2018 regardless of storm activity. Due to much less spatial coverage of Van Allen Probes at $L > 6.5$, we focus on the results at $L \leq 6.5$. The acceleration events are automatically selected using the following criteria:

1. The electron fluxes are first binned into a 0.1L×6 hr UT grid during 2013–2018. Due to the highly elliptical orbit of Van Allen Probes with orbit period of ∼9 hr, the time bin size of 6 hr ensures at least one available measurement in each bin for most of the time, which has been widely used to investigate the outer belt electron dynamics in previous studies (e.g., Hua, Bortnik, Chu, et al., 2022; Turner et al., 2015, 2019).
2. An increase of flux by a factor of >5 compared to the fluxes observed anytime within a 2-day look-back time window is considered as one acceleration sample, which captures the quick and significant flux enhancements. Here, one acceleration sample corresponds to one acceleration point at a given L-shell and energy in one 6-hr time bin.
3. The acceleration samples at a given L-shell and energy that were observed within 1 day are considered as the same acceleration event. Since there can be oscillations in electron fluxes during one acceleration event, this criterion ensures that the acceleration event with flux oscillations is regarded as one continuous event instead of multiple separate events.

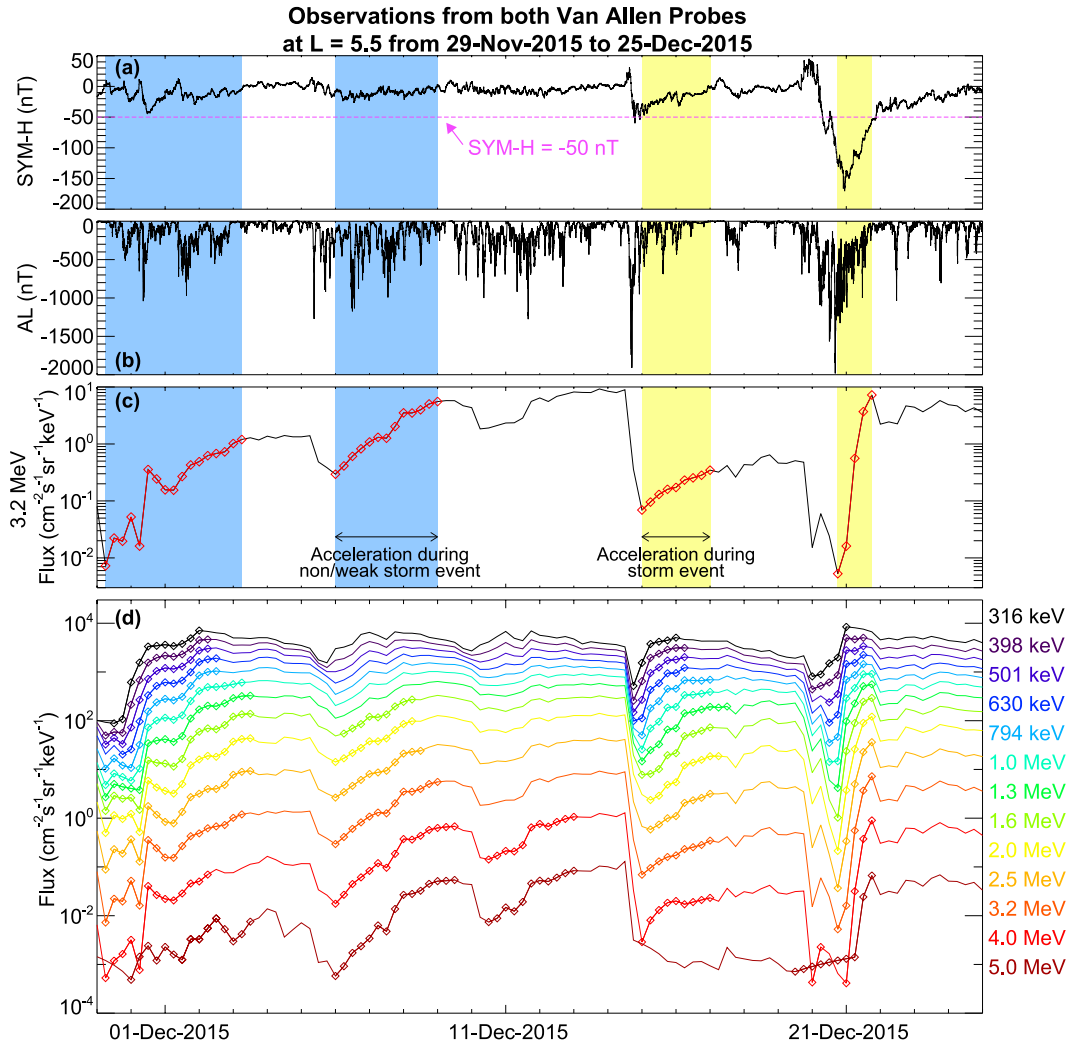

Figure 1. Examples of electron acceleration events observed at $L = 5.5$ by both Van Allen Probes. (a) SYM-H index, with the magenta dashed line representing SYM-H = −50 nT. (b) AL index. (c) Spin-averaged 3.2-MeV electron fluxes, with the red diamonds representing the selected acceleration events. The shaded regions in panels (a–c) correspond to acceleration events for 3.2-MeV electrons during non/weak storm (blue) and storm events (yellow), respectively. (d) Similar to (c) but for electron fluxes at color-coded energies, with the diamonds representing the identified acceleration events.

4. The commencement of the acceleration event (t_0) is defined as the time of the lowest flux within 2 days of look-back window of the first acceleration sample, while the end of the event (t_1) corresponds to the time of flux reaching its maximum value (j_{max}).

We use Van Allen Probes observations at $L = 5.5$ from 29 November to 25 December in 2015 to demonstrate how our selection criteria successfully identify acceleration events. The SYM-H and AL indices are show in Figures 1a and 1b. Figure 1c displays the 3.2-MeV electron fluxes, with all the fast and strong flux enhancements successfully identified as acceleration events, which are shown as red diamonds. Clearly, the acceleration events can be observed during both non/weak storm and storm times as highlighted in blue and yellow shaded regions, respectively. Here, the non/weak storm means the SYM-H index remains at >−50 nT during the whole acceleration event plus one day before t_0. Otherwise, it is considered to be a storm event. Therefore, we first identity the electron acceleration events and then determine their geomagnetic conditions so that the acceleration events are selected regardless of storm activity. Hereafter, $(\text{SYM-H})_{min}$ represents the minimum value of SYM-H during this time interval. Interestingly, all the four identified acceleration events seem to correlate with clusters of strong AL activity, suggesting the potentially important role of continuous substorms in these acceleration events. Furthermore, the identified acceleration events at color-coded energies in Figure 1d suggest that the acceleration

19448007, 2024, 13, Downloaded from https://agupubs.onlinelibrary.wiley.com/doi/10.1029/2024GL109612, Wiley Online Library on [25/05/2025]. See the Terms and Conditions (https://onlinelibrary.wiley.com/terms-and-conditions) on Wiley Online Library for rules of use; OA articles are governed by the applicable Creative Commons License

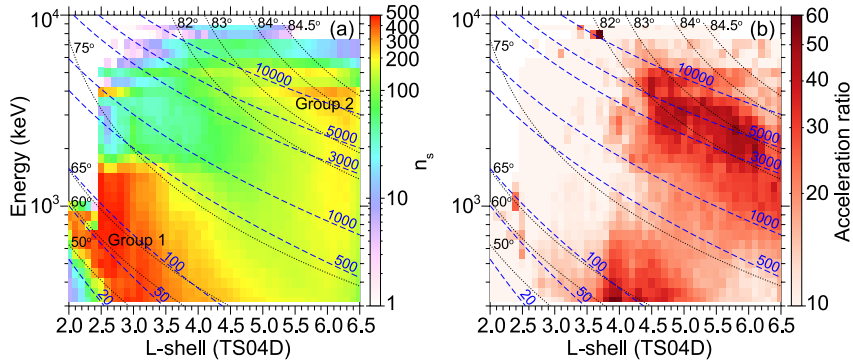

Figure 2. (a) Number of electron acceleration events as a function of L-shell and energy based on Van Allen Probes observations during 2013–2018. The black dotted lines represent the first-order cyclotron resonant energies of electrons at indicated pitch angles from 50° to 84.5° interacting with parallel propagating chorus waves at $0.25f_{ce}$ at the geomagnetic equator, while the blue dashed lines show the electron energies at indicated fixed μ from 20 to 10,000 MeV/G and fixed $K = 0.01\ G^{0.5}R_E$. (b) Similar to (a) but showing median results of acceleration ratio.

events strongly depend on energy, with different t_0, t_1, and magnitude of acceleration at different energies. Still, all the identified acceleration events at different energies are associated with clusters of strong AL index.

3. Results

3.1. Statistical Distributions of Electron Acceleration Events

Figure 2a shows the number of electron acceleration events as a function of L-shell and energy based on 6-years Van Allen Probes observations. Interestingly, it seems that the acceleration events fall into two groups as shown by the two peaks in number of acceleration events: one group at <~2 MeV at $L < 4.0$ (marked as Group 1 in Figure 2a), and another one at >~2 MeV at $L >$ ~4.5 (marked as Group 2 in Figure 2a). The distributions of the event numbers of both groups follow the trend of the characteristic energies resulting from the combined local acceleration by chorus waves and inward radial diffusion, suggesting that both acceleration mechanisms are important. Here, the black dotted lines represent the first-order cyclotron resonant energies of electrons at indicated pitch angles from 50° to 84.5° interacting with parallel propagating chorus waves at $0.25f_{ce}$ at the geomagnetic equator using plasma trough density model from Sheeley et al. (2001), while the blue dashed lines show the electron energies at indicated fixed μ from 20 to 10,000 MeV/G and fixed $K = 0.01\ G^{0.5}R_E$. Note that previous studies reported that chorus waves observed at extremely low L-shells ($L \sim 3.0$) can contribute to electron acceleration (Thorne et al., 2007; Zhang et al., 2020). Additionally, substorm injections can also contribute to outer belt electron acceleration (Dai et al., 2014; Kim et al., 2021, 2023; Tang et al., 2016). There are no acceleration events at $L <$ ~2.5 at energies >1 MeV, which is consistent with the impenetrable barrier to the outer belt ultrarelativistic electrons reported in previous study (Baker et al., 2014), and lack of observed MeV energies in the inner belt (Fennell et al., 2015).

Although the event numbers of Group 1 (with maximum number of >500) are much larger compared to those in Group 2 (reaching a maximum number of ~300), the overall acceleration ratio (Figure 2b) of Group 1 is smaller compared to Group 2. Here, acceleration ratio is defined as the ratio of the flux at t_1 over the flux at t_0, which describes the magnitude of the acceleration during the whole event. A larger acceleration ratio represents a stronger acceleration event. The median results over different events are shown in Figure 2b as a function of L-shell and energy. Similarly, the distribution of the acceleration ratio also follows the characteristic energies of combined local acceleration by chorus waves and inward radial diffusion. However, the acceleration ratio peaks at different regions as the event numbers, showing two peaks at $L >$ ~4.0, with overall larger ratio at >1 MeV compared to hundreds of keV electrons. One possible explanation is that the 100s keV electron fluxes can reach their saturation state with a timescale of several hours, while it takes longer for multi-MeV electrons to reach their upper limit of acceleration, which is typically several days (Hua, Bortnik, & Ma, 2022). Therefore, the multi-MeV electron fluxes can be continuously elevated during strong acceleration events, leading to larger acceleration ratio. There is a sharp drop in acceleration ratio at $L \sim 3.5$ at almost all energies. This can be attributed to the much less effective acceleration at low L-shells compared to higher L-shells, which is a combined result of much weaker

19448007, 2024, 13, Downloaded from https://agupubs.onlinelibrary.wiley.com/doi/10.1029/2024GL109612, Wiley Online Library on [25/05/2025]. See the Terms and Conditions (https://onlinelibrary.wiley.com/terms-and-conditions) on Wiley Online Library for rules of use; OA articles are governed by the applicable Creative Commons License

19448007, 2024, 13, Downloaded from https://agupubs.onlinelibrary.wiley.com/doi/10.1029/2024GL109612, Wiley Online Library on [25/05/2025]. See the Terms and Conditions (https://onlinelibrary.wiley.com/terms-and-conditions) on Wiley Online Library for rules of use; OA articles are governed by the applicable Creative Commons License

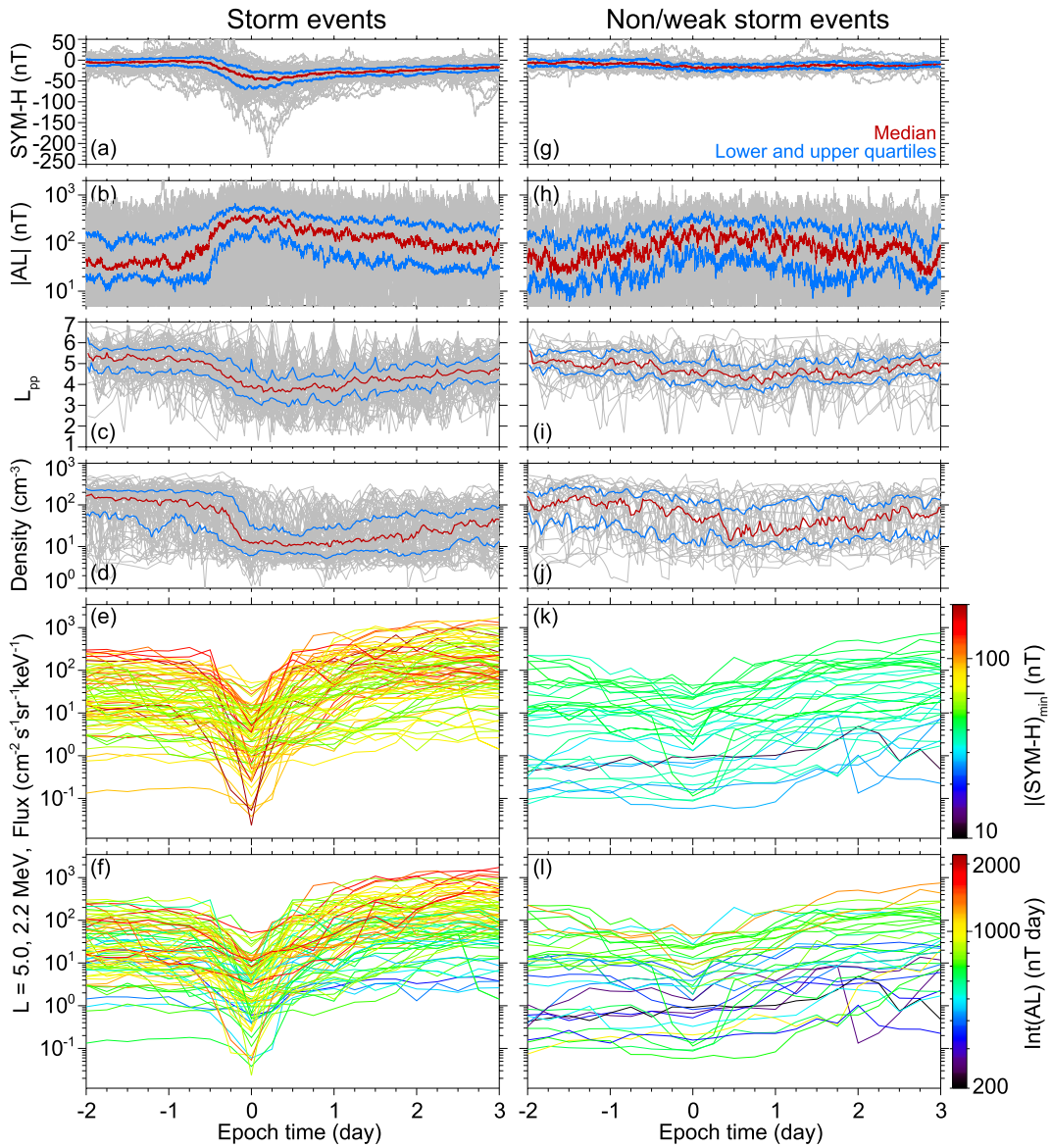

Figure 3. Comparison of superposed epoch analysis of acceleration events for 2.2-MeV electrons at $L = 5.0$ during (a–f) storm and (g–l) non/weak storm events. Note that $t_{epoch} = 0$ corresponds to the commencement of each acceleration event. (a) SYM-H index; (b) absolute value of AL index; (c) L-shell of the plasmapause location (L_{pp}); (d) Electron density. Here, the red lines show the median profile, while the blue lines represent the lower and upper quartiles. Electron fluxes at 2.2 MeV color-coded by the corresponding (e) $|(SYM\text{-}H)_{min}|$ and (f) Int(AL) in each acceleration event. (g–l) Similar to (a–f) but for non/weak storm events.

chorus wave intensities, particularly inside the plasmasphere (Aryan et al., 2021) and slower inward radial diffusion at $L < \sim 3.5$ (Brautigam & Albert, 2000). The results of the lower and upper quartile of the acceleration ratio are provided in Figure S1 in the supporting information, which demonstrate similar variation trend.

3.2. Determining the Critical Controlling Geomagnetic Activity Factors

Figure 3 presents a comparison of superposed epoch analysis of 2.2-MeV electron acceleration events near the heart of the outer belt at $L = 5.0$ during storm and non/weak storm events. Here, $t_{epoch} = 0$ corresponds to t_0, that is, the commencement of each acceleration event. We exclude the acceleration events after March 2018 due to the unavailability of AL measurements from OMNI data. The first two rows show the SYM-H and absolute value of AL (i.e., |AL|) indices. Although the overall |AL| value is slightly higher during storm compared to non/weak

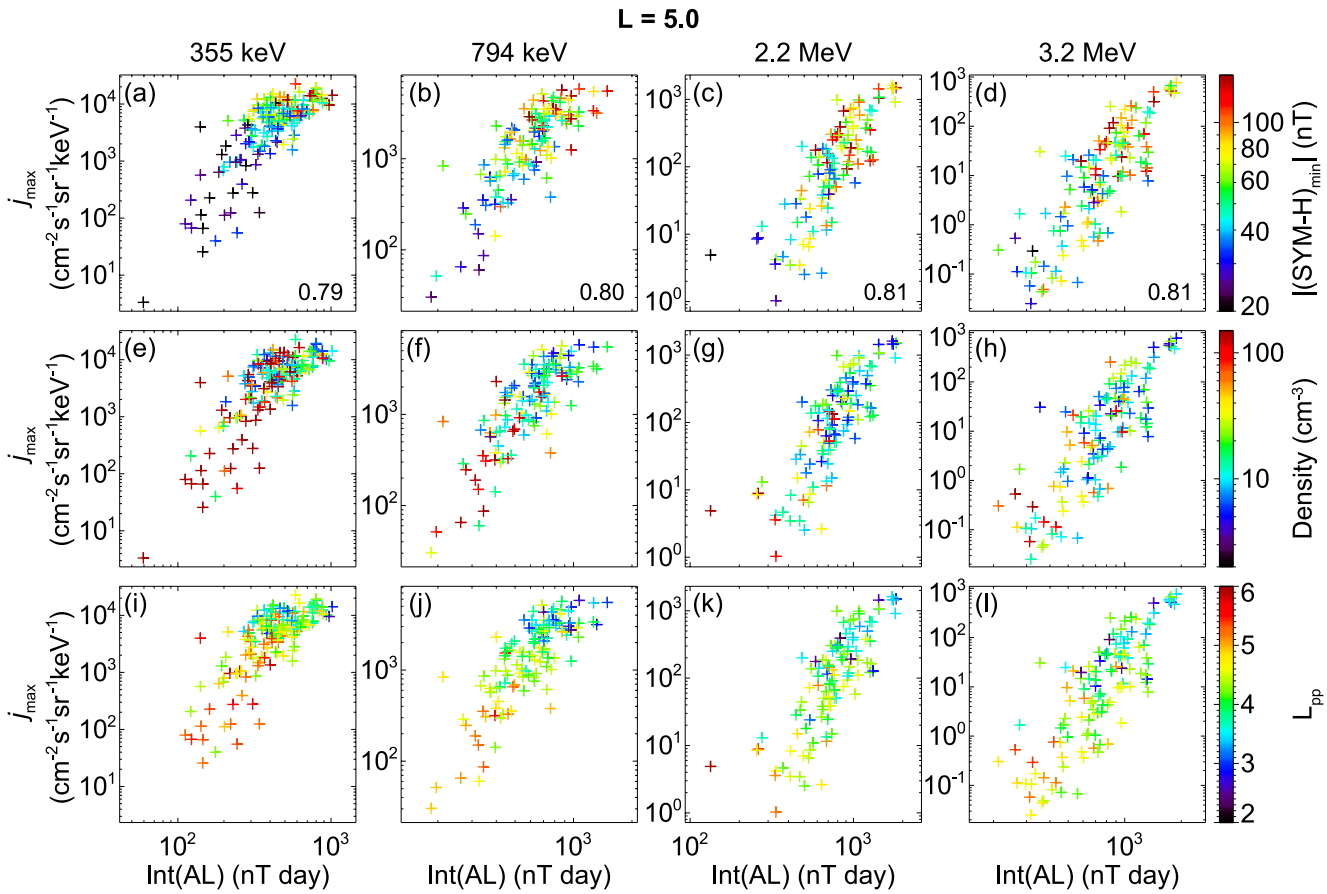

Figure 4. (a–d) Maximum electron fluxes (j_{max}) at $L = 5.0$ at indicated energies, from left to right: 355 keV, 794 keV, 2.2 MeV, and 3.2 MeV, versus the corresponding Int(AL) on the horizontal axis color-coded by the corresponding |(SYM-H)$_{min}$|, with the correlation coefficients between j_{max} and Int(AL) both in logarithm marked on the bottom left. Each plus symbol represents an individual acceleration event. (e–h) and (i–l) Similar to (a–d) but for the results color-coded by the corresponding median results of electron density and L_{pp} in each event, respectively.

storm events, the prolonged and intense increases in the |AL| index were observed during both storm and non/weak storm acceleration events. The third row shows the L-shell of the plasmapause location (L_{pp}) inferred from electron density data from Electric and Magnetic Field Instrument Suite and Integrated Science (EMFISIS; Kletzing et al., 2013) onboard both spacecrafts. The satellite is considered to be outside the plasmapause when the observed electron density is smaller than either 50 cm^{-3} or the value from the plasma trough model of Sheeley et al. (2001). We record the lowest L-shell when the satellite was in the plasma trough region as L_{pp} for each inbound and outbound trajectory. During storm events, due to the compression of the magnetosphere, the L_{pp} is pushed to lower L-shells near $t_{epoch} = 0$ accompanied with a clear decrease in electron density (Figure 3d), which are favorable for the efficient local acceleration by chorus waves (Allison et al., 2021; Hua, Bortnik, Kellerman, et al., 2023). In contrast, there is no significant variation in L_{pp} and electron density during non/weak storm acceleration events. Figures 3e and 3k present the 2.2-MeV electron fluxes color-coded by the corresponding absolute value of (SYM-H)$_{min}$, demonstrating that the electron acceleration is not well correlated with |(SYM-H)$_{min}$|. For example, even a weak storm with small |(SYM-H)$_{min}$| as shown by the green color can lead to a large maximum flux during the acceleration event. However, the electron acceleration is better organized by the time-integral of AL index (Int(AL)), with the larger Int(AL) almost always resulting in higher maximum fluxes (Figures 3f and 3l). Here, the Int(AL) is the integral of the |AL| during the time interval from t_0-dt to t_1, where dt corresponds to 2 days. Note that the Int(AL) shown in Figure 4 is calculated in the similar way.

The strong correlation between Int(AL) and j_{max} is demonstrated more clearly in Figure 4a–4d, showing the maximum fluxes (j_{max}) of electron acceleration events at energies from ~300 keV to 3.2 MeV versus Int(AL) on the horizontal axis, color-coded by the corresponding |(SYM-H)$_{min}$|. Clearly, there is a strong correlation between

19448007, 2024, 13, Downloaded from https://agupubs.onlinelibrary.wiley.com/doi/10.1029/2024GL109612, Wiley Online Library on [25/05/2025]. See the Terms and Conditions (https://onlinelibrary.wiley.com/terms-and-conditions) on Wiley Online Library for rules of use; OA articles are governed by the applicable Creative Commons License

19448007, 2024, 13, Downloaded from https://agupubs.onlinelibrary.wiley.com/doi/10.1029/2024GL109612, Wiley Online Library on [25/05/2025]. See the Terms and Conditions (https://onlinelibrary.wiley.com/terms-and-conditions) on Wiley Online Library for rules of use; OA articles are governed by the applicable Creative Commons License

j_{max} and Int(AL) with correlation coefficient (CC) reaching >0.8. A larger Int(AL) almost always leading to a higher j_{max}, confirming the important role of continuous and intense substorms in producing j_{max} for outer belt electron acceleration. We note that our results do not heavily depend on the choice of *dt*, which still have similar trend but with slightly lower or higher CC with *dt* varying from 0 to 3 days. On the contrary, a larger j_{max} is not necessarily associated with a stronger storm as measured by $(SYM\text{-}H)_{min}$. For instance, a moderate storm (as shown in green color) can lead to a j_{max} close to the highest upper limit of j_{max} during the 6-years observations. Nevertheless, the acceleration events during strong storms (shown in red color) seem to correlate with large Int(AL). These events are mostly associated with small electron density <∼20 cm^{-3} (Figure 4e–4h) and L_{pp} pushed to very low L-shells (Figure 4i–4l) that are favorable for local acceleration by chorus waves (Allison et al., 2021) compared to weak storm events with larger density and L_{pp}. Additionally, the enhanced inward radial diffusion during storms can also contribute to electron acceleration (Ozeke et al., 2020). Therefore, strong storms compared to non/weak storms can provide favorable conditions for electron acceleration, but they are not necessarily required in producing a large j_{max}, which is dominantly controlled by continuous and intense substorms.

4. Conclusions and Discussions

We comprehensively investigate the statistical distribution of the outer belt electron acceleration events over energies of 300 keV–10 MeV using 6-years observations from Van Allen Probes. By performing superposed epoch analysis of acceleration events during storm and non/weak storm events and comparing their geomagnetic conditions, we reveal the strong correlation between continuous and intense substorms as measured by Int(AL) and the upper limit of electron acceleration (j_{max}), while strong storms are not necessarily required to produce large maximum fluxes. To our best knowledge, this study provides the first statistical analysis of electron acceleration events regardless of storm activity during the whole Van Allen Probes Era, which is important to improve the way to investigate and organize the outer belt electron dynamics. Our results demonstrate the linear correlation between Int(AL) and j_{max}, which can be of great practical importance in future forecasting the extreme case of radiation belt environment. Our major conclusions are summarized as follows:

1. The statistical distributions of electron acceleration events in terms of event numbers and acceleration ratio strongly depend on L-shell and energy, whose variations follow the trend of the characteristic energies of both local acceleration by chorus waves and inward radial diffusion. While the event numbers fall into two groups with Group 1 at <∼2 MeV at $L < 4.0$ and Group 2 at >∼2 MeV at $L >$ ∼4.5, the acceleration ratio exhibit two peaks at $L >$ ∼4.0, with overall stronger acceleration at >1 MeV compared to hundreds of keV electrons.
2. The upper limit of outer belt electron fluxes is dominantly controlled by the cumulative effects of substorms, with strong CC between Int(AL) and j_{max} near the heart of the outer belt at $L = 5.0$ reaching >0.8.
3. Electron acceleration events can be observed during both storm and non/weak storm time. Although stronger storms are not necessarily linked with larger j_{max}, both smaller electron density and lower plasmapause location that can result in efficient local acceleration, and enhanced inward radial diffusion during intense storm activities are favorable for a more significant electron acceleration.

Although we investigated the statistical distributions of electron acceleration events that cover the whole outer belt over $L = 2.5$–6.5, we mostly focus on revealing the significant role of Int(AL) on the upper limit of acceleration events near the heart of the outer belt. It is worth noting that electron acceleration events can be frequently observed at $L <$ ∼4.0 below ∼2 MeV with event numbers >∼400 but small acceleration ratio. Since chorus wave intensities significant decrease at $L < 3.5$ (Aryan et al., 2021), chorus waves are less likely to cause these frequent acceleration events. Although inward radial diffusion may be a promising candidate to accelerate electrons at such low L-shells, this can only be achieved if radial diffusion coefficients from empirical model (e.g., Ozeke et al., 2014) are highly amplified (Hua et al., 2019). Future studies are needed to comprehensively investigate their acceleration mechanisms and controlling geomagnetic conditions.

Data Availability Statement

The ECT data were obtained from https://rbsp-ect.newmexicoconsortium.org/data_pub/. The electron density data from the EMFISIS instrument onboard Van Allen Probes were obtained from https://emfisis.physics.uiowa.edu/Flight. The geomagnetic indices were obtained from the OMNI data set (https://omniweb.gsfc.nasa.gov/ow_

min.html). The source data used to produce figures in the present study are publicly available at (Hua & Bortnik, 2024).

Acknowledgments
We acknowledge the Van Allen Probes mission, particularly the ECT team for providing the particle data and EMFISIS team for providing the electron density data. We gratefully acknowledge the OMNI team. The authors gratefully acknowledge subgrant 1559841 to the University of California, Los Angeles, from the University of Colorado Boulder under NASA Prime Grant agreement 80NSSC20K1580 and NSF GEM award 2025706 and 2247255.

References

Agapitov, O., Mourenas, D., Artemyev, A., Hospodarsky, G., & Bonnell, J. W. (2019). Time scales for electron quasi-linear diffusion by lower-band chorus waves: The effects of ωpe/Ωce dependence on geomagnetic activity. *Geophysical Research Letters*, *46*(12), 6178–6187. https://doi.org/10.1029/2019GL083446

Allison, H. J., Shprits, Y. Y., Zhelavskaya, I. S., Wang, D., & Smirnov, A. G. (2021). Gyroresonant wave-particle interactions with chorus waves during extreme depletions of plasma density in the Van Allen radiation belts. *Science Advances*, *7*(5), eabc0380. https://doi.org/10.1126/sciadv.abc0380

Anderson, B. R., Millan, R. M., Reeves, G. D., & Friedel, R. H. W. (2015). Acceleration and loss of relativistic electrons during small geomagnetic storms. *Geophysical Research Letters*, *42*(23), 10113–10119. https://doi.org/10.1002/2015GL066376

Aryan, H., Bortnik, J., Meredith, N. P., Horne, R. B., Sibeck, D. G., & Balikhin, M. A. (2021). Multi-parameter chorus and plasmaspheric hiss wave models. *Journal of Geophysical Research: Space Physics*, *126*(1), e2020JA028403. https://doi.org/10.1029/2020JA028403

Baker, D., Jaynes, A., Hoxie, V., Thorne, R. M., Foster, J. C., Li, X., et al. (2014). An impenetrable barrier to ultrarelativistic electrons in the Van Allen radiation belts. *Nature*, *515*(7528), 531–534. https://doi.org/10.1038/nature13956

Boyd, A. J., Reeves, G. D., Spence, H. E., Funsten, H. O., Larsen, B. A., Skoug, R. M., et al. (2019). RBSP-ECT combined spin-averaged electron flux data product. *Journal of Geophysical Research: Space Physics*, *124*(11), 9124–9136. https://doi.org/10.1029/2019JA026733

Brautigam, D. H., & Albert, J. M. (2000). Radial diffusion analysis of outer radiation belt electrons during the October 9, 1990, magnetic storm. *Journal of Geophysical Research*, *105*(A1), 291–309. https://doi.org/10.1029/1999JA900344

Dai, L., Wygant, J. R., Cattell, C. A., Thaller, S., Kersten, K., Breneman, A., et al. (2014). Evidence for injection of relativistic electrons into the earth's outer radiation belt via intense substorm electric fields. *Geophysical Research Letters*, *41*(4), 1133–1141. https://doi.org/10.1002/2014GL059228

Fennell, J. F., Claudepierre, S. G., Blake, J. B., O'Brien, T. P., Clemmons, J. H., Baker, D. N., et al. (2015). Van Allen probes show that the inner radiation zone contains no MeV electrons: ECT/MagEIS data. *Geophysical Research Letters*, *42*(5), 1283–1289. https://doi.org/10.1002/2014GL062874

Gu, X., Xia, S., Fu, S., Xiang, Z., Ni, B., Guo, J., & Cao, X. (2020). Dynamic responses of radiation belt electron fluxes to magnetic storms and their correlations with magnetospheric plasma wave activities. *The Astrophysical Journal*, *891*(2), 127. https://doi.org/10.3847/1538-4357/ab71fc

Hua, M., & Bortnik, J. (2024). Upper limit of outer belt electron acceleration and their controlling geomagnetic conditions: A comparison of storm and non-storm events [Dataset]. *Figshare*. https://doi.org/10.6084/m9.figshare.25513525

Hua, M., Bortnik, J., Chu, X., Aryan, H., & Ma, Q. (2022). Unraveling the critical geomagnetic conditions controlling the upper limit of electron fluxes in the earth's outer radiation belt. *Geophysical Research Letters*, *49*(22), e2022GL101096. https://doi.org/10.1029/2022GL101096

Hua, M., Bortnik, J., Kellerman, A. C., Camporeale, E., & Ma, Q. (2023). Ensemble modeling of radiation belt electron acceleration by chorus waves: Dependence on key input parameters. *Space Weather*, *21*(3), e2022SW003234. https://doi.org/10.1029/2022SW003234

Hua, M., Bortnik, J., & Ma, Q. (2022). Upper limit of outer radiation belt electron acceleration driven by whistler-mode chorus waves. *Geophysical Research Letters*, *49*(15), e2022GL099618. https://doi.org/10.1029/2022GL099618

Hua, M., Bortnik, J., Spence, H. E., & Reeves, G. D. (2023). Testing the key processes that accelerate outer radiation belt relativistic electrons during geomagnetic storms. *Frontiers in Astronomy and Space Sciences*, *10*, 1168636. https://doi.org/10.3389/fspas.2023.1168636

Hua, M., Li, W., Ma, Q., Ni, B., Nishimura, Y., Shen, X.-C., & Li, H. (2019). Modeling the electron flux enhancement and butterfly pitch angle distributions on L shells <2.5. *Geophysical Research Letters*, *46*(20), 10967–10976. https://doi.org/10.1029/2019GL084822

Hudson, M. K., Kress, B. T., Mueller, H.-R., Zastrow, J. A., & Blake, J. B. (2008). Relationship of the Van Allen radiation belts to solar wind drivers. *Journal of Atmospheric and Solar-Terrestrial Physics*, *70*(5), 708–729. https://doi.org/10.1016/j.jastp.2007.11.003

Jaynes, A. N., Baker, D. N., Singer, H. J., Rodriguez, J. V., Loto'aniu, T. M., Ali, A. F., et al. (2015). Source and seed populations for relativistic electrons: Their roles in radiation belt changes. *Journal of Geophysical Research: Space Physics*, *120*(9), 7240–7254. https://doi.org/10.1002/2015JA021234

Kim, H.-J., Lee, D.-Y., Wolf, R., Bortnik, J., Kim, K.-C., Lyons, L., et al. (2021). Rapid injections of MeV electrons and extremely fast step-like outer radiation belt enhancements. *Geophysical Research Letters*, *48*(9), e2021GL093151. https://doi.org/10.1029/2021GL093151

Kim, H.-J., Noh, S. J., Lee, D. Y., Lyons, L., Bortnik, J., Nagai, T., et al. (2023). Can strong substorm-associated MeV electron injections be an important cause of large radiation belt enhancements? *Frontiers in Astronomy and Space Sciences*, *10*, 1128923. https://doi.org/10.3389/fspas.2023.1128923

Kletzing, C. A., Kurth, W. S., Acuna, M., MacDowall, R. J., Torbert, R. B., Averkamp, T., et al. (2013). The electric and magnetic field instrument suite and integrated science (EMFISIS) on RBSP. *Space Science Reviews*, *179*(1–4), 127–181. https://doi.org/10.1007/s11214-013-9993-6

Li, W., Ma, Q., Thorne, R. M., Bortnik, J., Zhang, X. J., Li, J., et al. (2016). Radiation belt electron acceleration during the 17 March 2015 geomagnetic storm: Observations and simulations. *Journal of Geophysical Research: Space Physics*, *121*(6), 5520–5536. https://doi.org/10.1002/2016JA022400

Ma, D., Bortnik, J., Ma, Q., Hua, M., & Chu, X. (2024). Machine learning interpretability of outer radiation belt enhancement and depletion events. *Geophysical Research Letters*, *51*(1), e2023GL106049. https://doi.org/10.1029/2023GL106049

Mauk, B. H., Fox, N. J., Kanekal, S. G., Kessel, R. L., Sibeck, D. G., & Ukhorskiy, A. (2013). Science objectives and rationale for the radiation belt storm probes mission. *Space Science Reviews*, *179*(1–4), 3–27. https://doi.org/10.1007/s11214-012-9908-y

Mourenas, D., Agapitov, O. V., Artemyev, A. V., & Zhang, X.-J. (2022). A climatology of long-duration high 2-MeV electron flux periods in the outer radiation belt. *Journal of Geophysical Research: Space Physics*, *127*(8), e2022JA030661. https://doi.org/10.1029/2022JA030661

Mourenas, D., Artemyev, A. V., & Zhang, X.-J. (2019). Impact of significant time-integrated geomagnetic activity on 2-MeV electron flux. *Journal of Geophysical Research: Space Physics*, *124*(6), 4445–4461. https://doi.org/10.1029/2019JA026659

Murphy, K. R., Watt, C. E. J., Mann, I. R., Jonathan Rae, I., Sibeck, D. G., Boyd, A. J., et al. (2018). The global statistical response of the outer radiation belt during geomagnetic storms. *Geophysical Research Letters*, *45*(9), 3783–3792. https://doi.org/10.1002/2017GL076674

O'Brien, T. P., McPherron, R. L., Sornette, D., Reeves, G. D., Friedel, R., & Singer, H. J. (2001). Which magnetic storms produce relativistic electrons at geosynchronous orbit? *Journal of Geophysical Research*, *106*(A8), 15533–15544. https://doi.org/10.1029/2001JA000052

19448007, 2024, 13, Downloaded from https://agupubs.onlinelibrary.wiley.com/doi/10.1029/2024GL109612, Wiley Online Library on [25/05/2025]. See the Terms and Conditions (https://onlinelibrary.wiley.com/terms-and-conditions) on Wiley Online Library for rules of use; OA articles are governed by the applicable Creative Commons License

Ozeke, L. G., Mann, I. R., Dufresne, S. K. Y., Olifer, L., Morley, S. K., Claudepierre, S. G., et al. (2020). Rapid outer radiation belt flux dropouts and fast acceleration during the March 2015 and 2013 storms: The role of ULF wave transport from a dynamic outer boundary. *Journal of Geophysical Research: Space Physics*, *125*(2), e2019JA027179. https://doi.org/10.1029/2019JA027179

Ozeke, L. G., Mann, I. R., Murphy, K. R., Jonathan Rae, I., & Milling, D. K. (2014). Analytic expressions for ULF wave radiation belt radial diffusion coefficients. *Journal of Geophysical Research: Space Physics*, *119*(3), 1587–1605. https://doi.org/10.1002/2013JA019204

Reeves, G. D. (1998). Relativistic electrons and magnetic storms: 1992–1995. *Geophysical Research Letters*, *25*(11), 1817–1820. https://doi.org/10.1029/98GL01398

Reeves, G. D., McAdams, K. L., Friedel, R. H. W., & O'Brien, T. P. (2003). Acceleration and loss of relativistic electrons during geomagnetic storms. *Geophysical Research Letters*, *30*(10), 1529. https://doi.org/10.1029/2002GL016513

Reeves, G. D., Spence, H. E., Henderson, M. G., Morley, S. K., Friedel, R. H. W., Funsten, H. O., et al. (2013). Electron acceleration in the heart of the Van Allen radiation belts. *Science*, *341*(6149), 991–994. https://doi.org/10.1126/science.1237743

Sheeley, B. W., Moldwin, M. B., Rassoul, H. K., & Anderson, R. R. (2001). An empirical plasmasphere and trough density model: CRRES observations. *Journal of Geophysical Research*, *106*(A11), 25631–25641. https://doi.org/10.1029/2000JA000286

Spence, H. E., Reeves, G. D., Baker, D. N., Blake, J. B., Bolton, M., Bourdarie, S., et al. (2013). Science goals and overview of the radiation belt storm probes (RBSP) energetic particle, composition, and thermal plasma (ECT) suite on NASA's Van Allen Probes mission. *Space Science Reviews*, *179*(1–4), 311–336. https://doi.org/10.1007/s11214-013-0007-5

Tang, C. L., Zhang, J.-C., Reeves, G. D., Su, Z. P., Baker, D. N., Spence, H. E., et al. (2016). Prompt enhancement of the earth's outer radiation belt due to substorm electron injections. *Journal of Geophysical Research: Space Physics*, *121*(12), 11826–11838. https://doi.org/10.1002/2016JA023550

Thorne, R. M., Li, W., Ni, B., Ma, Q., Bortnik, J., Chen, L., et al. (2013). Rapid local acceleration of relativistic radiation-belt electrons by magnetospheric chorus. *Nature*, *504*(7480), 411–414. https://doi.org/10.1038/nature12889

Thorne, R. M., Shprits, Y. Y., Meredith, N. P., Horne, R. B., Li, W., & Lyons, L. R. (2007). Refilling of the slot region between the inner and outer electron radiation belts during geomagnetic storms. *Journal of Geophysical Research*, *112*(A6), A06203. https://doi.org/10.1029/2006JA012176

Tsyganenko, N. A., & Sitnov, M. I. (2005). Modeling the dynamics of the inner magnetosphere during strong geomagnetic storms. *Journal of Geophysical Research*, *110*(A3), A03208. https://doi.org/10.1029/2004JA010798

Tu, W., Cunningham, G. S., Chen, Y., Morley, S. K., Reeves, G. D., Blake, J. B., et al. (2014). Event-specific chorus wave and electron seed population models in DREAM3D using the Van Allen Probes. *Geophysical Research Letters*, *41*(5), 1359–1366. https://doi.org/10.1002/2013GL058819

Turner, D. L., Kilpua, E. K. J., Hietala, H., Claudepierre, S. G., O'Brien, T. P., Fennell, J. F., et al. (2019). The response of Earth's electron radiation belts to geomagnetic storms: Statistics from the Van Allen Probes era including effects from different storm drivers. *Journal of Geophysical Research: Space Physics*, *124*(2), 1013–1034. https://doi.org/10.1029/2018JA026066

Turner, D. L., O'Brien, T. P., Fennell, J. F., Claudepierre, S. G., Blake, J. B., Kilpua, E. K. J., & Hietala, H. (2015). The effects of geomagnetic storms on electrons in Earth's radiation belts. *Geophysical Research Letters*, *42*(21), 9176–9184. https://doi.org/10.1002/2015GL064747

Zhang, K., Li, X., Zhao, H., Xiang, Z., Khoo, L. Y., Zhang, W., et al. (2021). Upper limit of electron fluxes observed in the radiation belts. *Journal of Geophysical Research: Space Physics*, *126*(1), e2020JA028511. https://doi.org/10.1029/2020JA028511

Zhang, Z., Chen, L., Liu, S., Xiong, Y., Li, X., Wang, Y., et al. (2020). Chorus acceleration of relativistic electrons in extremely low L-shell during geomagnetic storm of August 2018. *Geophysical Research Letters*, *47*(4), e2019GL086226. https://doi.org/10.1029/2019GL086226

Zhao, H., Baker, D. N., Li, X., Malaspina, D. M., Jaynes, A. N., & Kanekal, S. G. (2019). On the acceleration mechanism of ultrarelativistic electrons in the center of the outer radiation belt: A statistical study. *Journal of Geophysical Research: Space Physics*, *124*(11), 8590–8599. https://doi.org/10.1029/2019JA027111

19448007, 2024, 13, Downloaded from https://agupubs.onlinelibrary.wiley.com/doi/10.1029/2024GL109612, Wiley Online Library on [25/05/2025]. See the Terms and Conditions (https://onlinelibrary.wiley.com/terms-and-conditions) on Wiley Online Library for rules of use; OA articles are governed by the applicable Creative Commons License